



Effects of Ultralow Temperature and Water Saturation on the Mechanical Properties of Sandstone

Decheng Zhang¹ · Guanju Lu¹ · Jie Wu¹ · Wen Nie¹ · P. G. Ranjith²

Received: 16 August 2022 / Accepted: 8 January 2023 / Published online: 30 January 2023
© The Author(s), under exclusive licence to Springer-Verlag GmbH Austria, part of Springer Nature 2023

Abstract

The surrounding rocks are subjected to ultralow temperatures in applications like liquid nitrogen fracturing, underground storage of liquefied natural gas and polar constructions etc. The mechanical properties of sandstone with different saturations under freezing temperature and after one ultralow temperature freeze–thaw cycle test conditions were investigated in this study. The uniaxial compressive strength (UCS) of both dry and saturated samples increases with the decrease in temperature except at $-90\text{ }^{\circ}\text{C}$ under freezing temperature test conditions, while the UCS of saturated samples is lower than that of dry samples after one ultralow temperature freeze–thaw cycle due to the water softening effects and the damage induced during the water–ice phase transition. The failure patterns of dry samples are more complex than those of saturated samples under freezing temperature, which is also indicated in the lower brittleness index for the saturated samples. The ice cohesion effect and its creep deformation increase the plastic deformation, while decreasing the Young’s modulus of saturated samples under freezing temperature. In addition, the ice net formed in the connected pores significantly increases the sample tensile strength and makes its failure less severe. The UCS, Young’s modulus and brittleness index decrease with saturation under $-120\text{ }^{\circ}\text{C}$, while the tensile strength increases with saturation. Porosity reduction measured by computerized tomography for the saturated samples after one freeze–thaw cycle is largest at $-120\text{ }^{\circ}\text{C}$ compared with those at $-60\text{ }^{\circ}\text{C}$ and $-180\text{ }^{\circ}\text{C}$, which is certified by the pore filling shown in scanning electron microscope images.

Highlights

- Tensile strength is more sensitive to the variations of subzero temperatures compared with the compression strength.
- The cohesion and creep deformation of ice increase the plastic deformation while decrease the elastic modulus.
- Porosity reduces after one freeze–thaw cycle due to pore filling.
- Compression strength and brittleness index decrease while tensile strength increases with the saturation under $-120\text{ }^{\circ}\text{C}$.
- Failure patterns of dry samples are more complex than those of saturated samples under low temperatures.

Keywords Ultralow temperature · Freeze–thaw · Mechanical properties · Brittleness · Water–ice phase transition

1 Introduction

Rocks are subjected to ultralow temperatures in various cryogenic rock engineering processes (Fig. 1), such as liquid nitrogen fracturing (LNG, $-196\text{ }^{\circ}\text{C}$) in tight oil and gas

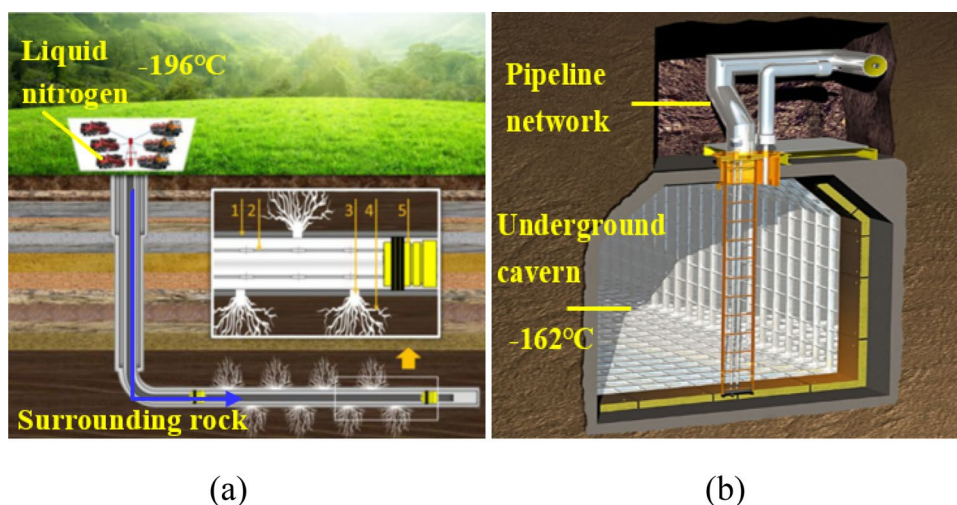
reservoirs (Li et al. 2016), liquefied natural gas ($-162\text{ }^{\circ}\text{C}$) and liquid air ($-193\text{ }^{\circ}\text{C}$) storage in rock caverns (Xu et al. 2013; He et al. 2019; Looney. 2021) and constructions in severe cold and polar regions (Feng et al. 2014). The mechanical responses of rocks under such extreme temperature conditions are important for the safety and stability of these projects. Hydraulic fracturing is an effective technique to stimulate the tight oil, gas and geothermal reservoirs. However, there are several issues in the conventional hydraulic fracturing practices, such as excessive water consumption, formation damage and contamination of flowback fluids. Liquid nitrogen fracturing as an alternative is suitable

✉ Jie Wu
jie.voo@gmail.com

¹ School of Civil and Transportation Engineering, Hebei University of Technology, Tianjin 300401, China

² Department of Civil Engineering, Monash University, Building 60, Melbourne, VIC 3800, Australia

Fig. 1 **a** Liquid nitrogen fracturing (Li et al. 2016); **b** underground LNG storage (Chung et al. 2006)



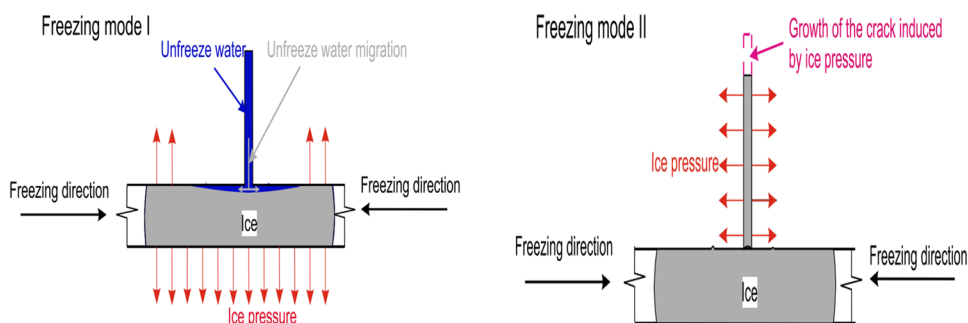
for water shortage areas and water-sensitive reservoirs. The temperature of the surrounding rocks during the liquid nitrogen fracturing is between $-196\text{ }^{\circ}\text{C}$ and reservoir temperature, and rock damage is induced by the thermal stress and fluid phase change, etc. Therefore, it is of great significance to investigate the rock mechanical properties under different ultralow temperature and saturation conditions.

Experiments on rock mechanical responses under freezing temperature conditions were conducted by some researchers. Matsunaga et al. (1981) found that the compressive strength of dry granite increased from 200 to 280 MPa when the temperature decreased from 20 to $-180\text{ }^{\circ}\text{C}$, while its tensile strength remained almost constant. The compressive strength of saturated granite increased from 130 to 230 MPa and its tensile strength increased from 6 to 12 MPa. Mardoukhi et al. (2020) found the tensile strength of saturated granite fluctuated with the reduction of temperature, which was 20 MPa, 33 MPa and 26 MPa at $20\text{ }^{\circ}\text{C}$, $-30\text{ }^{\circ}\text{C}$ and $-70\text{ }^{\circ}\text{C}$, respectively. The strength increase at freezing temperatures is due to particle shrinkage, pore closure and increases in rock cohesion and internal friction angle for dry rocks, while the pore filling and bonding effect caused by ice for saturated rocks further enhances the bearing capacity (Kammoshida et al. 2010). Kodama et al. (2013) showed that

the compressive and tensile strengths of tuffs and andesites increased with water saturation at $-20\text{ }^{\circ}\text{C}$. Kammoshida et al. (2010) found that the compressive strength of saturated sandstone was lower than that of dry sandstone at $20\text{ }^{\circ}\text{C}$, but its strength at $-170\text{ }^{\circ}\text{C}$ was higher for saturated sandstone, which implies that the strength enhancement is more significant for saturated sandstone than for dry samples.

Inada and Yokota (1984) measured the compressive and tensile strengths of granite and andesite after one ultralow temperature freeze–thaw cycle, and the results showed that the rock strength decreased with the reduction of treatment temperature. Since the mineral particles will shrink/expand with the decrease/increase of temperature, the discrepancies of thermal expansion coefficients between different minerals result in thermal stress, which increases with the cooling or heating amplitude. When the thermal stress exceeds the cohesion strength between particles, cracks will be formed, so the ultralow temperature will induce irreversible damage. Cai et al. (2014a, b) froze the dry and water-saturated sandstones, marbles and shales with liquid nitrogen and analyzed the sample scanning electron microscope (SEM) and nuclear magnetic resonance (NMR) results before and after freezing. The results indicated that the pore number and volume of the dry sandstone increase after the liquid nitrogen treatment

Fig. 2 Schematics of two modes of water mitigation, freeze and expansion (Jia et al. 2020)



due to its large mineral and pore size, while the interparticle fractures become more obvious for the compact marble and shale. Water-saturated samples demonstrated more damage with larger microfractures due to the volumetric expansion in the water–ice phase transition. Memon et al. (2020) found the shale fracture size and permeability increased with the liquid nitrogen immersion time.

Jia et al. (2016, 2020) analyzed the freezing damage mechanisms of sandstone and pointed out that water in the primary crack first freezes, followed by two potential freezing damage modes (Fig. 2): (1) the unfrozen water in the secondary crack migrates and freezes in the stem crack, which induces the freezing stress and expansion of the stem crack; (2) unfrozen water migrates and freezes in the secondary crack leading to the secondary crack extension.

Huang et al. (2020) proposed a freezing damage model for the dual pore structure, which incorporated the pore size distribution, effect of unfrozen water film and the interfacial free energy, and further investigated the influence of unfrozen water film thickness on the separation pressure and frost heaving strain. Ming et al. (2021) built a Weibull damage distribution constitutive model to describe the damage evolution in frozen rock based on the triaxial compression tests under ultralow temperatures. Bai et al. (2020) developed a frozen rock statistical damage model for the void compaction and deformation at residual stress stages based on the Weibull damage distribution (Weibull 1951), the Lemaitre strain equivalence principle and the triaxial stress–strain curves (Lemaitre 1985). Xie et al. (2014) used Gaussian peak function to fit the energy absorption curve of frozen soil and established a dynamic constitutive frozen soil model, which can better reflect the stress–strain responses under impact loading. Ning et al. (2005) studied the frozen rock characteristics from the perspective of mesoscopic mechanics of composite materials and derived the equivalent elastic modulus of frozen soil mixtures. An elastic constitutive model of damaged frozen rock was also built. Li and Wang (2012) established a frozen rock model incorporating the coefficients of thermal stress and the ice expansion force based on the nonlinear thermoelastic theory with variable physical parameters, and the determination of thermal stress coefficients with temperature under uniaxial compression conditions was also introduced.

Although the rock freezing damage has been studied by many scholars, most studies are for temperatures above -40 °C with few focusing on the ultralow temperature conditions (-200 to -40 °C). Besides, many researchers only investigated some specific ultralow temperatures such as -196 °C in liquid nitrogen immersion; thus, a full-scale ultralow temperature range study is needed. In addition, samples subjected to the ultralow temperature treatment in literature are either in dry or fully saturated condition, while rocks are

usually in partial water saturation conditions. Therefore, it is necessary to investigate the mechanical properties of partially saturated rocks under ultralow temperatures.

Tight sandstone was used in this study, as it is usually the reservoir rock for unconventional oil and gas resources. The dry and water-saturated Sichuan Zigong sandstones with a porosity of 8.38% were subjected to a series of ultralow temperatures from -30 to -180 °C, and samples with different saturations were frozen at -120 °C. Then uniaxial compression and Brazilian tensile strength (BTS) tests were conducted under freezing temperature and after one freeze–thaw cycle test conditions, and the pore structure changes before and after the ultralow temperature treatments were analyzed by computerized tomography (CT) and scanning electron microscope (SEM). The effects of ultralow temperature treatments and water saturation conditions on the rock mechanical and microstructure properties are analyzed in detail.

2 Experimental Methods

2.1 Sample Preparation

The sample is caesious sandstone from Zigong, Sichuan Province, China. The bedding structure is not obvious and the dry density of the sample is 2460 kg/m³. The sample mineral composition was tested by the X-ray diffraction (XRD) equipment (Rigaku Smartlab 9kw, Japan) in Hebei University of Technology. The test power was 4 kW and the scanning angle was 5 – 90 ° with a speed of 6 °/min. The Zigong sandstone is composed by 60.4% albite, 30.1% quartz, 6.5% calcite and small amounts of other minerals such as clinocllore and muscovite as shown in Fig. 3. The pore size distribution was measured by the mercury intrusion test (Micromeritics AutoPore IV 9500) with a maximum filling pressure of 40,000 psia and a contact angle of 130 °. The sample porosity is 8.38% with the pore size mainly distributed between 0.005 and 350 μ m as shown in Fig. 4. The properties of the sandstone used in the experiments are shown in Table 1.

Samples were first cored from the blocks, then cut and ground to standard cylinders with dimensions of $\Phi 50 \times 100$ mm and $\Phi 50 \times 25$ mm for uniaxial compression and Brazilian tensile strength tests, respectively, as shown in Fig. 5. The unevenness of the end surface is less than 0.25 mm, while its departure from the perpendicularity is within 0.25 °, which satisfy the requirements of ISRM (Ulusay 2015).

Dry samples were prepared by placing the samples in an oven at 105 °C until the difference between two successive mass measurements (every 4 h) was less than 0.1%. The samples were then cooled to room temperature and wrapped

Fig. 3 **a** X-ray diffraction pattern; **b** mineral composition of sandstone

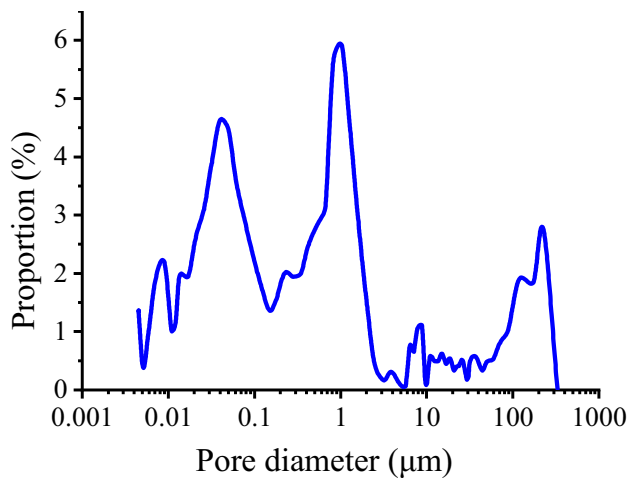
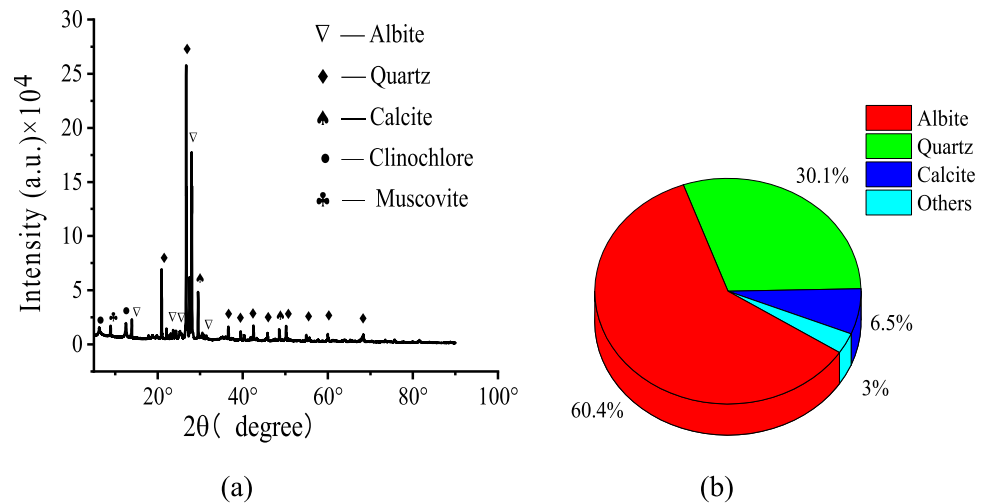


Fig. 4 Pore size distribution of sandstone

with a cling wrap. Vacuum saturation method was used to fully saturate the sandstone sample. Samples were placed in a vacuum chamber, and water was injected to the chamber slowly after it was fully vacuumed. Once the samples were fully immersed in water, they were weighed every 12 h until the mass difference between two successive measurements was less than 0.1%. Then cling wrap was used to prevent the water evaporation of saturated samples. The partial saturated samples were prepared according to the weight of adsorbed water. Samples were first fully saturated and weighed, and then they were completely dried in an oven at 105 °C. The

water content at full saturation was calculated, from which the target water contents at 25%, 50% and 75% saturations were calculated. Then these samples were put into the water chamber and taken out every 1 min to weigh until they reached the target masses with 25%, 50% and 75% saturations. Water spray and sample evaporation were conducted to reach the exact saturation level. Finally, the partial saturated samples were wrapped with the cling wrap and kept in a container at room temperature for 30 days for the uniform moisture distribution. The sample mass was weighed again before freezing and no change was found.

2.2 Sample Low Temperature Treatment

The wrapped dry and saturated rock samples were frozen at -30 °C, -60 °C, -90 °C and -120 °C in a compressor freezer (Guangdong Aoxue DW-150W42), while liquid nitrogen cryogenic chamber (Shanghai Gawler GL-50 N) was used for freezing at -150 °C and -180 °C. The partial saturated samples were frozen in the compressor freezer at -120 °C. The cooling rate was 2 °C/min and the samples were kept at the target temperature for 12 h for all the freezing treatments. A dummy sample with a thermocouple buried in the drilled hole at the sample center was used to measure the variations of the sample center temperature during the freezing process under different ultralow temperatures as shown in Fig. 6c, d. The diameter and depth of the hole were 5 mm and 52 mm, respectively. The sample center temperature was delayed in reaching

Table 1 Properties of dry Zigong sandstone

Properties	ρ (g/cm ³)	ϕ (%)	UCS (MPa)	BTS (MPa)	E (GPa)	k (m ²)	V_p (km/s)	V_s (km/s)
Value	2.43	8.38	87.2	5.9	16.2	$8.6e-15$	3.521	1.450

ρ , density; ϕ , porosity; UCS, uniaxial compressive strength; BTS, Brazilian tensile strength; E , elastic modulus; k , permeability (Liu et al. 2014); V_p , P -wave velocity; V_s , S -wave velocity (Wan et al. 2020)

Fig. 5 Samples for **a** uniaxial compression test and **b** Brazilian tensile test

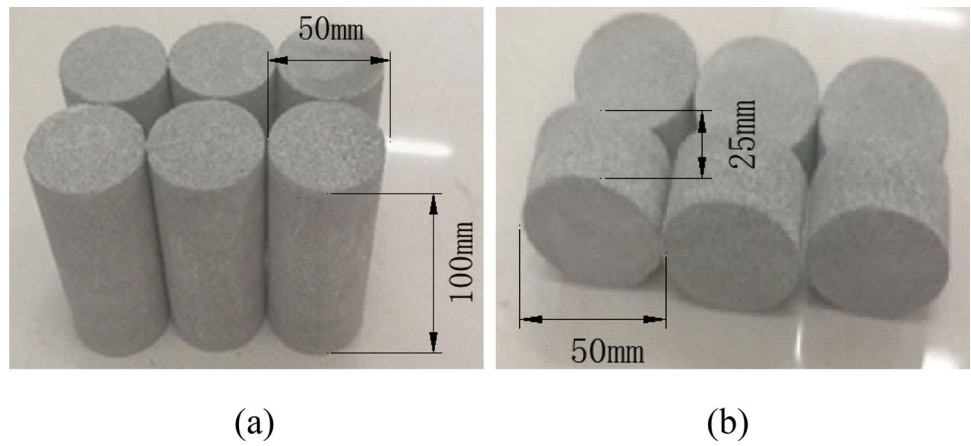
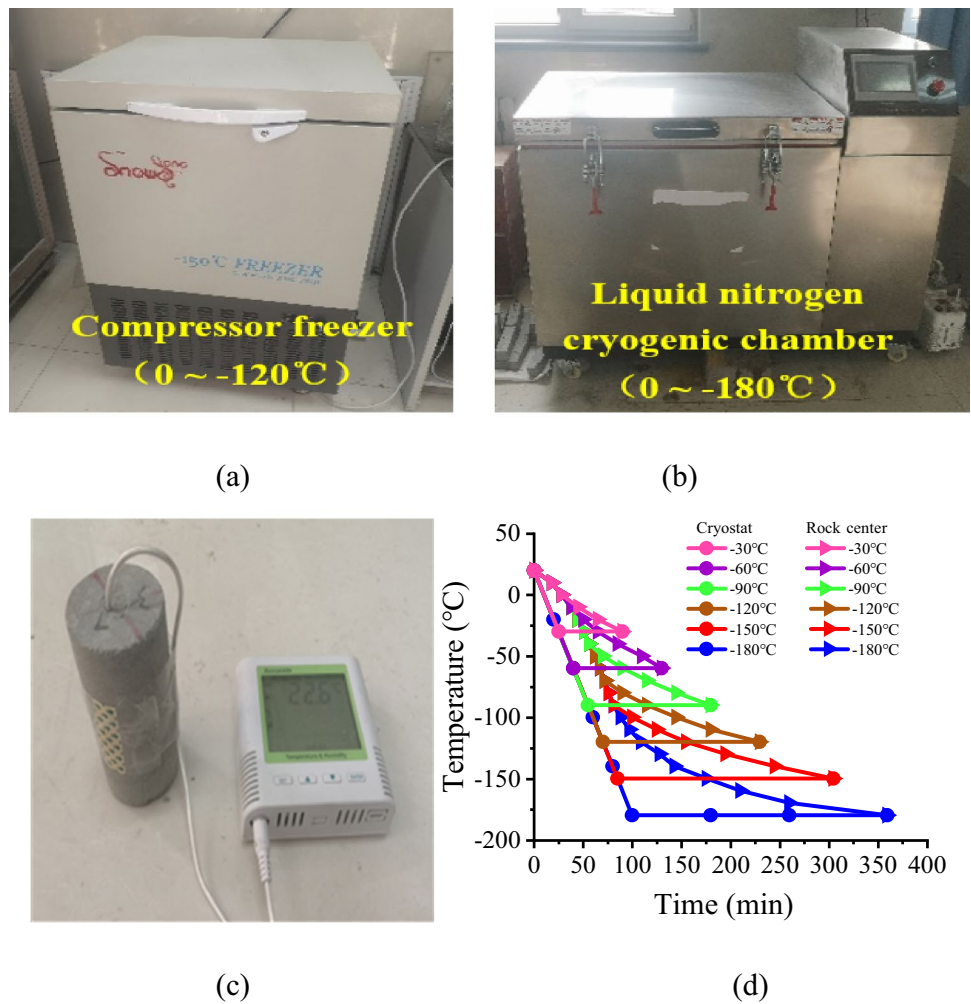


Fig. 6 Test equipment and temperature measurement, **a** compressor freezer; **b** liquid nitrogen cryogenic chamber; **c** sample center temperature measurement; **d** cooling curves



the target ultralow temperatures than the cryogenic chamber temperature. Therefore, the holding time at the target temperature was used for the whole sample to be fully frozen. Some samples were taken out from the cryostat

and wrapped with the asbestos for the tests under freezing temperature conditions. The other samples were left in the cryostat to gradually return to the room temperature for the tests after one freeze–thaw cycle.

Fig. 7 MTS system and sample wrapped by the asbestos



2.3 Uniaxial Compression and Brazilian Tensile Strength Tests

A hydraulic servo-controlled Materials Test Systems (MTS, Landmark 370.5, USA) with a maximum load of 500 kN and an accuracy of 10^{-6} kN was used for our tests. The room temperature was controlled at 20 °C by an air conditioner. Samples were wrapped by the asbestos and compressed immediately after taking out from the freezer for the freezing temperature tests as shown in Fig. 7. The loading rate was 0.2 mm/min for all the tests, and the load and displacement were monitored by MTS. Three samples were tested under each condition. Equations (1) and (2) were used to calculate the compressive and tensile strengths, respectively.

$$\sigma_c = \frac{4P}{\pi D^2}, \quad (1)$$

where σ_c is the compressive strength, D is the sample diameter and P is the peak load.

$$\sigma_t = \frac{2P}{\pi DH}, \quad (2)$$

where σ_t is the tensile strength and H is the sample thickness.

2.4 Microscopic Tests

The sample microstructure changes before and after the ultralow temperature treatments were observed by using the FF35 X-ray CT (YXLON, Germany) and the JSM 7610F scanning electron microscope (JEOL, Japan). The saturated samples with a dimension of $\Phi 7 \times 15$ mm were scanned before and after freezing at -60 °C, -120 °C and -180 °C. The voltage and current for the X-ray tube were 200 V and 230 A, respectively. The number of scanned slices was 1080 with an image resolution of 2146×2146 . The scanned data were analyzed by using the VGSTUDIO software. The sample thin slices were saturated and frozen at -150 °C. The

SEM scanning of sample thin slices was conducted before and after the ultralow temperature treatment.

3 Results and Analysis

3.1 UCS After the Cryogenic Treatments

3.1.1 Stress–Strain Curve Analysis

The stress–strain curves of dry and saturated sandstones tested under freezing temperature and after one freeze–thaw cycle conditions are shown in Fig. 8.

Researchers have developed many models to fit the stress–strain curves, including the composite power-exponential nonlinear model (Wang et al. 2017) and the viscoelastic–plastic model (Zhu and Zhang 1992) etc. Wang et al. (2021) further improved the viscoelastic–plastic model by introducing the relationship between failure strain and temperature as shown below:

$$\sigma/\sigma_{\max} = \left[\frac{\varepsilon}{\varepsilon_t} \right]^n \exp \left[n \left(1 - \frac{\varepsilon}{\varepsilon_t} \right) \right], \quad (3)$$

$$\varepsilon_t = a \cdot \exp(-b|T|), \quad (4)$$

where σ is the stress, σ_{\max} is the peak strength, ε is the strain, ε_t is the total strain at failure, T is the temperature and a , b and n are coefficients.

These two equations are used to fit the stress–strain data of the saturated samples under different freezing temperatures. The model curves fit well with the experimental data as shown in Fig. 9. The corresponding curve fitting parameters are listed in Table 2. Both n and b decrease with the reduction of temperature.

The uniaxial compression stress–strain curve can be divided into four stages (Fig. 10): compaction stage, elastic stage, plastic stage and failure stage (Feng et al. 2022). The corresponding strains for the stages before failure are crack

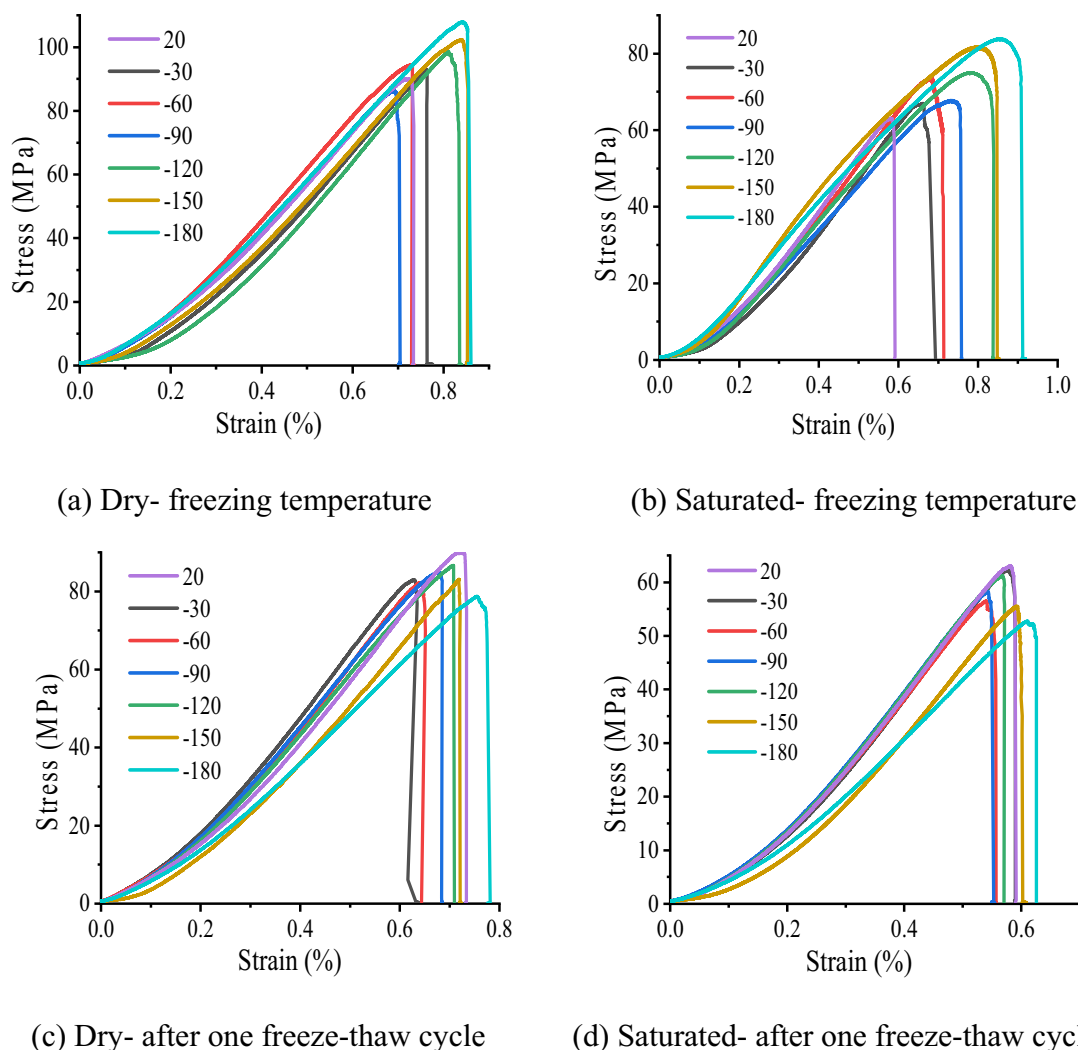


Fig. 8 Stress–strain curves under freezing temperature (a, b) and after one freeze–thaw cycle (c, d) conditions

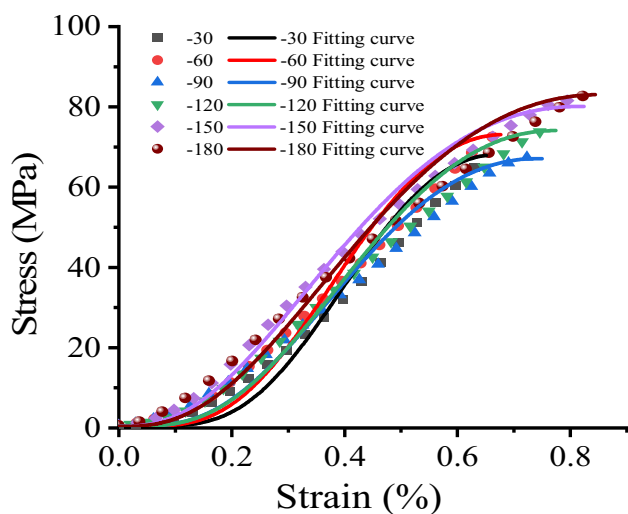


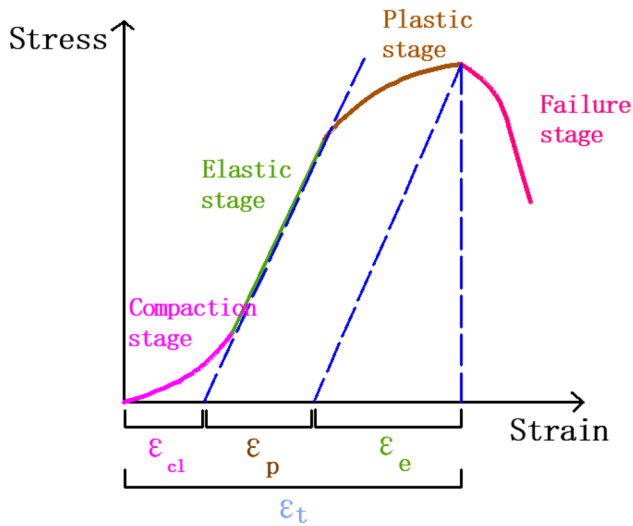
Fig. 9 Stress–strain data and fitting curves for saturated samples at different freezing temperatures

closure strain (ϵ_{cl}), elastic strain (ϵ_e) and plastic strain (ϵ_p), while their summation is the total strain at failure (ϵ_t). Strain variations with the temperature at different test and saturation conditions are shown in Fig. 11.

The crack closure strain ranges from 0.08 to 0.23%, which generally reduces with the decrease of temperature. For tests under freezing temperature conditions, the shrinkage of pre-existing cracks and the pore filling and expansion due to the water–ice phase transition result in the decrease of crack closure strain, especially for the saturated samples. While for tests after one freeze–thaw cycle, the gentle reduction in the crack closure strain indicates that the one-time freeze–thaw treatment causes little damage to the sample and the irreversible shrinkage strain induces the reduction of crack closure strain. The elastic strain ranges from 0.4 to 0.7% accounting for the most part of the total strain. The elastic strains for dry samples are higher than those for saturated

Table 2 Stress–strain curve fitting parameters

$T/^\circ\text{C}$	σ_{\max}/MPa	$\varepsilon_l/\%$	n	a	b	R^2
–30	68.212	0.673	5.18	–0.88	1.52	0.982
–60	73.331	0.684	4.98	–0.54	1.41	0.981
–90	67.242	0.7405	3.95	–1.40	1.34	0.984
–120	74.734	0.7735	3.95	–0.14	1.31	0.990
–150	80.556	0.814	2.83	0.25	1.25	0.994
–180	83.838	0.8535	2.99	0.23	1.21	0.987

**Fig. 10** Different stages and strains in the uniaxial compression stress–strain curve

samples, and tests under freezing temperature conditions have larger elastic strains compared with those tested after one freeze–thaw cycle. These findings are consistent with the strength behaviours which are also higher under dry and freezing temperature test conditions. All the elastic strains increase as the temperature decreases. The contraction and ice filling increase the elastic strain under freezing temperature conditions, while the plastic strain fluctuates around 0.03% except for the saturated samples under freezing temperature conditions. Saturated samples can endure larger plastic strains at lower temperatures due to the increasing cohesion of ice. As the total strain is mainly composed of elastic strain, its variations at failure follow the same trends as those of elastic strains. Besides, the relative standard deviation of the total strain is less than 5%, which is much smaller than those of other strains values.

3.1.2 UCS and Young's Modulus

Figure 12 shows the changes of compressive strength and Young's modulus with decreasing temperature under different test conditions. The Young's modulus is the slope of the elastic stage on the stress–strain curve. Their relative

standard deviations are both less than 6%, which shows the high accuracy of the measured data. Table 3 summarizes the variation trends and corresponding mechanisms.

Under freezing temperature test conditions, variations of the compressive strengths of dry and saturated sandstones follow the same pattern with strengths of dry samples being higher than those of saturated samples. This is due to the softening effects of water and ice between particles compared with the direct particle contacts. The UCS of dry and saturated sandstones increased by 8.23% and 17.22%, respectively, when the temperature decreased from 20 to -60°C . The thermal shrinkage made the sample more compact, which increased the UCS for both dry and saturated samples. The water freezing point gradually decreases with the reduction of pore diameter and the bound water has a lower freezing point than that of free water (Sammis and Biegel 2004; Jia et al. 2019). Therefore, the pore water gradually froze at 0 to -60°C , which increased the bearing area and the cohesion between particles resulting in the higher sensitivity for the saturated rocks (Tang et al. 2010; Chen et al. 2004; Kurilko and Novopashin 2005). Besides, the strength of ice increases with the decrease of temperatures (Sammis and Biegel 2004; Haynes 1980). The UCS of dry and saturated sandstones decreased by 9.43% and 7.69%, respectively, when the temperature reduced from -60 to -90°C . Different thermal expansion coefficients between quartz and albite (Ma et al. 2021), which are the main constituent minerals of sandstone, induced the tensile and shear stress at the grain boundaries. When the stress exceeded the cohesion strength in the temperature range from -60 to -90°C , tensile or shear failure occurred resulting in the cracks at grain boundaries, destruction of cementing minerals and the relative grain movement toward the original defects in the sample. The deformations of grains and pores in the dry and saturated samples during the freeze–thaw cycle are shown in Fig. 13, which are certified by the UCS behaviors and the microscopic observations by CT and SEM as stated in Sect. 3.4. Therefore, the damage of solid skeleton induced the reductions of UCS for both dry and saturated samples. Though the volume expansion in the water–ice phase transition also induces some cracks near the pores, these new created cracks are filled and cemented by the

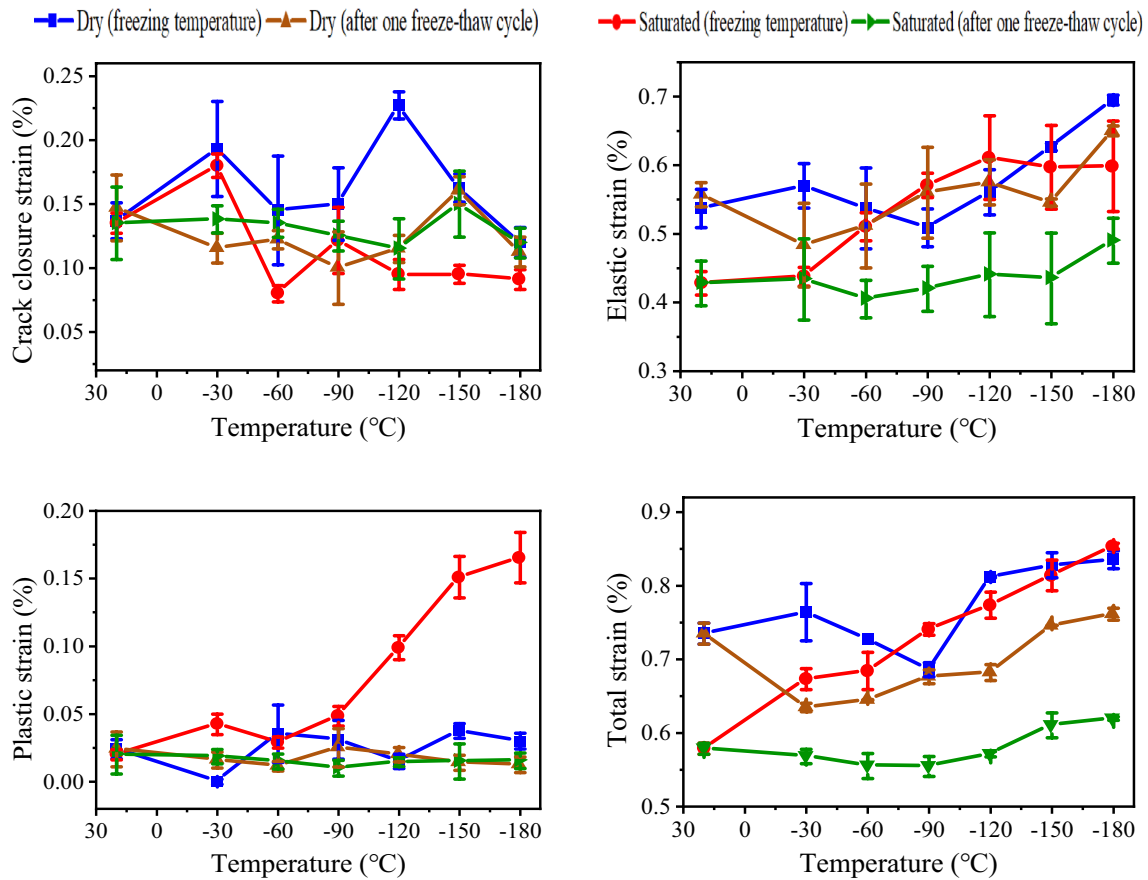
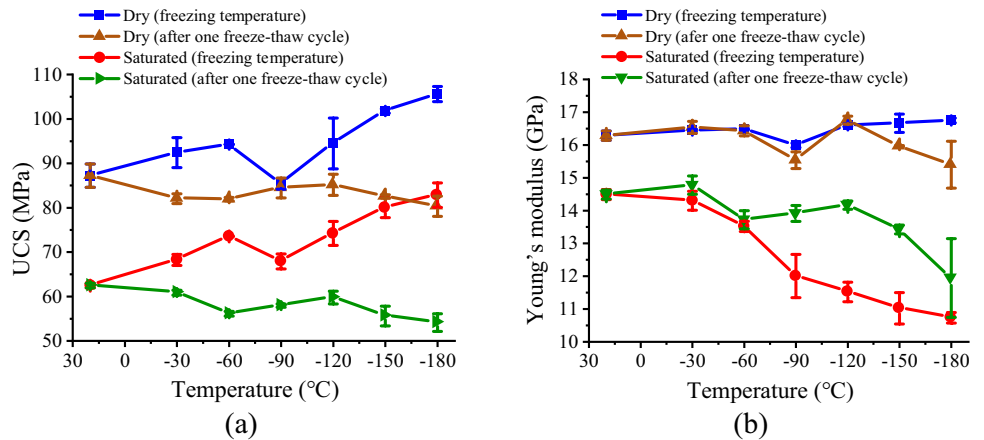


Fig. 11 Variations of crack closure strain, elastic strain, plastic strain and total strain at failure

Fig. 12 a Compressive strength and b elastic modulus



ice resulting in the smaller strength reduction under freezing temperatures. With the further temperature decrease to $-180\text{ }^{\circ}\text{C}$, the UCS of dry and saturated samples increased again due to the contractions of grains, pores and ice (Arakawa and Maeno 1997).

The Young's modulus of dry samples under freezing temperature test conditions has the same trend as its UCS but with a smaller variation magnitude, while the Young's

modulus of saturated samples are always lower than those of dry samples and reduce continuously with the decrease of temperature. The Young's modulus of saturated samples at $-180\text{ }^{\circ}\text{C}$ reduced by 25.97% compared with that at $20\text{ }^{\circ}\text{C}$. The reduction was caused by the increase of ice content initially, as the Young's modulus of ice is much smaller than those of rock minerals (Ji et al. 2011), while the larger thermal expansion coefficient of ice compared with those

Table 3 Variations of UCS under freezing temperature and after one freeze–thaw cycle

Test condition	Temperature	Change	Mechanisms
Under freezing temperature (dry and sat)	20 to –60 °C –60 to –90 °C	Increase Decrease	(1) Thermal shrinkage made the sample compact (2) Water gradually changed into ice and filled the pore (3) Strength of ice increases with the decrease of temperatures Tensile or shear damage occurs at the grain boundaries due to the different thermal expansion coefficients
After one freeze–thaw cycle (dry and sat)	–90 to –180 °C 20 to –60 °C	Increase Decrease	Contractions of grains, pores and ice (1) Irreversible damage caused by the discordant expansion between minerals (2) Volumetric changes during water–ice phase transitions
Comparisons	–60 to –120 °C –120 to –180 °C	Increase Decrease	(3) Water softening effects Pore filling by the destructed debris and the mineral deformation toward the pore The large shrinkage and expansion deformations of different minerals and the ice crystals induced greater damages
	(1) UCS of dry and saturated samples under freezing temperature follow the same pattern, but those of dry samples are higher due to the softening effects of water and ice in saturated samples compared with the direct mineral contacts (2) UCS of samples after one freeze–thaw cycle is lower than that of untreated samples due to the irreversible damage, while UCS under freezing temperature is higher than that of the untreated samples		

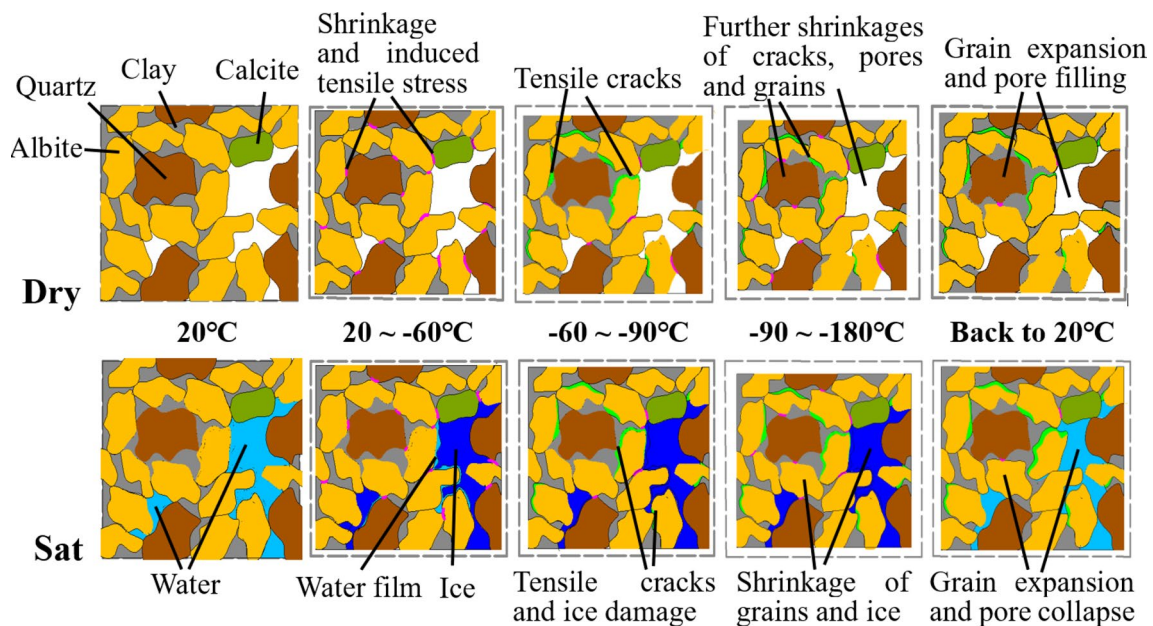


Fig. 13 Grain and pore deformations of dry and saturated samples during freeze–thaw cycle

of rock minerals increases the creep deformation inside the pores, which decreases the Young's modulus at freezing temperatures.

After one freeze–thaw cycle, the UCS of saturated samples have the same trend with those of the dry samples, but the UCS of the saturated samples are always lower at the same temperature. The water softening effects after one freeze–thaw cycle test condition (Zhang et al. 2017) and the water–ice phase transition-induced damage during the freeze–thaw cycle resulted in the lower strength of the saturated samples. In addition, the UCS of both dry and saturated samples subjected to one freeze–thaw cycle treatments is always lower than those of untreated samples due to the irreversible damage caused by the discordant expansion between minerals (Jia et al. 2013; Zhao et al. 2019) and the volumetric expansion in the water to ice phase transition (Song et al. 2020). The UCS of dry and saturated sandstones decreased by 6.1% and 10.3%, respectively, for the temperature from 20 to -60 °C due to irreversible damages, while the strengths increased for both dry and saturated samples as temperature decreased from -60 to -120 °C, which was also observed by Inada and Yokota (1984). As mentioned above, the tensile and shear failure occurred especially near large pores at around -90 °C resulting in the pore filling by the destroyed debris and the mineral deformation toward the large defects after the thawing process as shown in Fig. 13, which was also confirmed by the microscopic observations in Sect. 3.4. The pore filling increased the compressive strength. With the further decrease of subjected temperature of one freeze–thaw cycle to -180 °C, the UCS of dry and saturated samples decreased by 5.64% and 9.45%,

respectively. The large shrinkage and expansion deformations of different minerals and the ice crystals during the temperature cycle induced greater damages to the sample; therefore, the UCS decreased in this temperature range. The Young's modulus of dry samples was always higher than those of the saturated samples, and great declines were shown from -120 to -180 °C for both samples due to the large accumulated damage when subjected to the ultralow temperatures freeze–thaw cycle.

The UCS of both dry and saturated samples under freezing temperature test conditions was higher than its counterparts after one freeze–thaw cycle test condition, indicating the enhancement effect of freezing temperature on strength. The Young's modulus of dry samples after one freeze–thaw cycle is almost identical to those under freezing temperature when the temperature is above -120 °C, while they are much lower under -150 °C and -180 °C due to the large strength difference. The Young's modulus of saturated samples under freezing temperature conditions are always lower than those after one freeze–thaw cycle. This is because there are more direct grain contacts as water is discharged during compression after one freeze–thaw cycle compared with the ice-filled intergranular spaces under freezing temperature. The elastic modulus of ice is much smaller than those of rock minerals.

3.1.3 Failure Pattern

Figure 14 shows the sample failure patterns after the uniaxial compression tests under freezing temperature conditions. The failure patterns of dry samples are diagonal

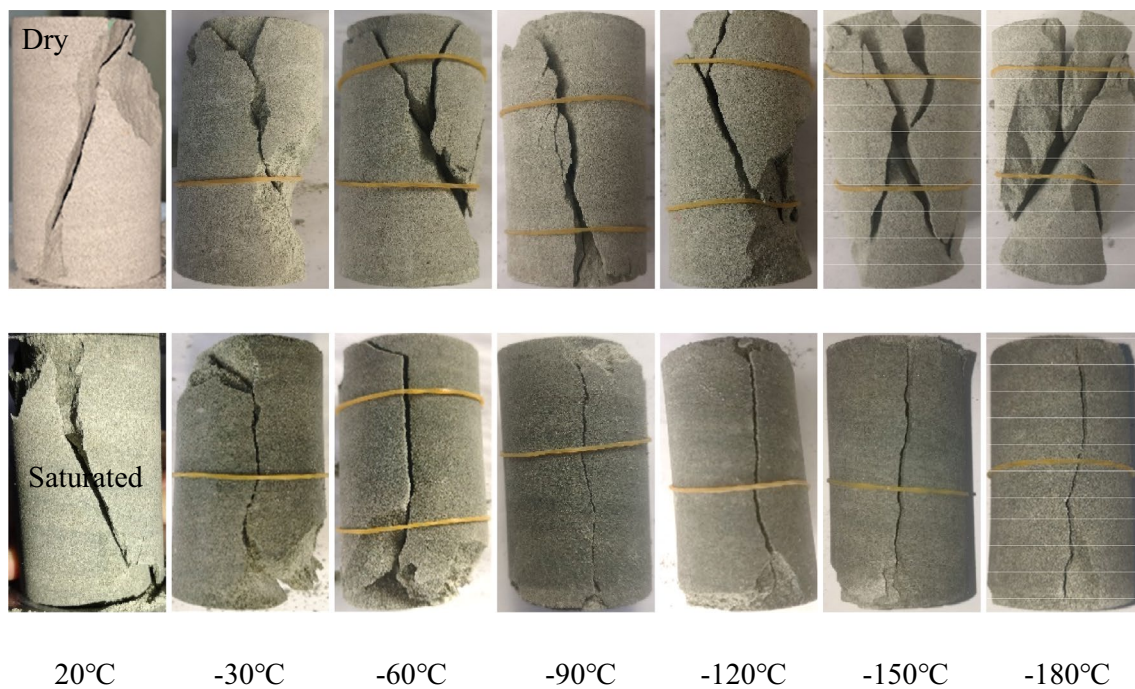


Fig. 14 UCS failure patterns of dry (upper row) and saturated (lower row) samples at different temperatures

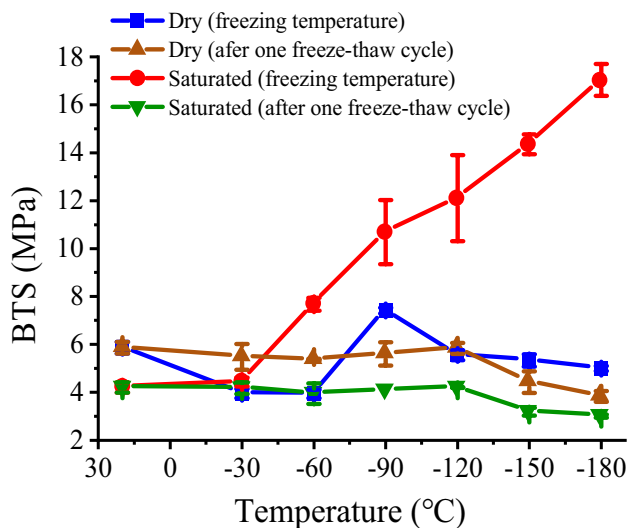


Fig. 15 Tensile strength under different conditions

shear at 20 °C, Y-type shear at -30 °C, -60 °C, -90 °C and -120 °C, and X-type shear at -150 °C and -180 °C. When referring to the strength of dry samples under freezing temperatures, the failure becomes violent with more macroscopic fractures for samples with higher strengths. While the failure patterns of saturated samples are diagonal shear at 20 °C, Z-type shear at -30 °C and -60 °C and vertical splitting shear at -90 °C, -120 °C, -150 °C and

-180 °C. Though the strength of saturated samples also increases with the decrease of temperature, the ice filling and cohesion effect make the sample more homogeneous resulting in the failure pattern change from oblique shear to vertical splitting. Compared with the saturated samples, the failure patterns are more complex for dry samples due to the high energy release upon destruction, as the strengths of dry samples are much higher than those of saturated samples.

3.2 Tensile Strength and Brittleness

3.2.1 Tensile Strength

Figure 15 shows the variations of sample tensile strength with temperature under different conditions with most of the relative standard deviations of the measured data being smaller than 10%. Table 4 summarizes the variation trends and the corresponding mechanisms. The tensile strength of dry sandstones under freezing temperature decreased from 5.86 MPa at 20–3.93 MPa at -60 °C, then it increased to 7.41 MPa at -90 °C, followed by a continuous decrease to 5.37 MPa at -180 °C. This variation trend was also reported by Matsunaga et al. (1981). The tensile stress generated by the external load was coupled with the thermal stress induced by the different shrinkage deformations of quartz and albite at -30 °C and -60 °C, which resulted in the reduction of tensile strength. The thermal stress exceeded the intergranular cohesion at -90 °C resulting in

Table 4 Variations of BTS under freezing temperature and after one freeze–thaw cycle

Test condition	Temperature	Change	Mechanisms
Under freezing temperature (dry)	20 to –60 °C	Decrease	The tensile stress generated by the external load was coupled with the thermal stress
	–60 to –90 °C	Increase	(1) The thermal stress-induced failure made the internal thermal stress disappear (2) The sample became more compact
Under freezing temperature (sat)	–90 to –180 °C	Decrease	The internal thermal stress and damage increased
	20 to –180 °C	Increase	(1) Ice content and strength increased with the decrease in temperature, which filled the pores and cemented the minerals (2) Ice net formed in the connected pores increased the tensile strength
After one freeze–thaw cycle (dry and sat)	20 to –120 °C –120 to –180 °C	Almost constant Decrease	Influences of thermal stress and ice disappear Significant damage induced at ultralow temperatures
Comparisons	The tensile strengths of saturated samples under freezing temperature are higher than those of dry samples due to the cohesion of ice, while the tensile strengths of saturated samples after one freeze–thaw cycle are lower than those of dry samples due to the water softening effect and freeze–thaw damage		

the relative movement between grains and the disappearance of the internal thermal stress. In addition, the sample became more compacted under –90 °C, which also contributed to the higher tensile strength. With the further temperature decrease, the internal thermal stress and accumulated damage increased again resulting in the reduction of tensile strength, while the tensile strength of saturated rock under freezing temperature increased continuously with the decrease of temperature with the strength at –180 °C being four times that at 20 °C. This is because the ice content and strength increased with the temperature decrease, which could fill the pores and cement the minerals. What is more, the ice in the connected pores formed an ice net, which significantly increased the tensile strength. The tensile strengths of saturated samples were higher than those of dry samples under subzero temperatures, and their differences increased as the temperature decreased.

For tests after one freeze–thaw cycle, the tensile strength of both dry and saturated samples was almost constant when the subjected temperature was higher than –120 °C, while obvious reductions were shown at –150 °C and –180 °C due to the significant damage induced at ultralow temperature freeze–thaw cycle. The tensile strengths of saturated samples were always lower than those of dry samples due to the water softening effect and damage in the water–ice phase transitions.

3.2.2 Failure Pattern

Figure 16 shows the fracture morphologies after the tensile failure under freezing temperature conditions. Bifurcations occurred at temperatures of 20 °C and –90 °C for dry samples. When referring to the tensile strengths of dry samples at different freezing temperatures, bifurcations were only shown for samples with high strengths, while bifurcations occurred at 20 °C for saturated samples, which corresponded to the lowest strength conditions. As the temperature decreased, no bifurcations were shown and the damaged area at the sample ends became smaller. In addition, the fracture became straighter at lower temperatures. This is because the bearing capacities of the sample defects were significantly enhanced due to the ice filling and cohesion effects, which increased the homogeneity and integrity of the sample. Therefore, the initiated fracture would propagate along a straight line without any branching.

3.2.3 Brittleness Index

Brittleness index is usually used to describe the deformation and failure characteristics including the strain, energy, strength and failure pattern. Zhang et al. (2016) summarized the brittleness indices for rocks, which can be obtained from

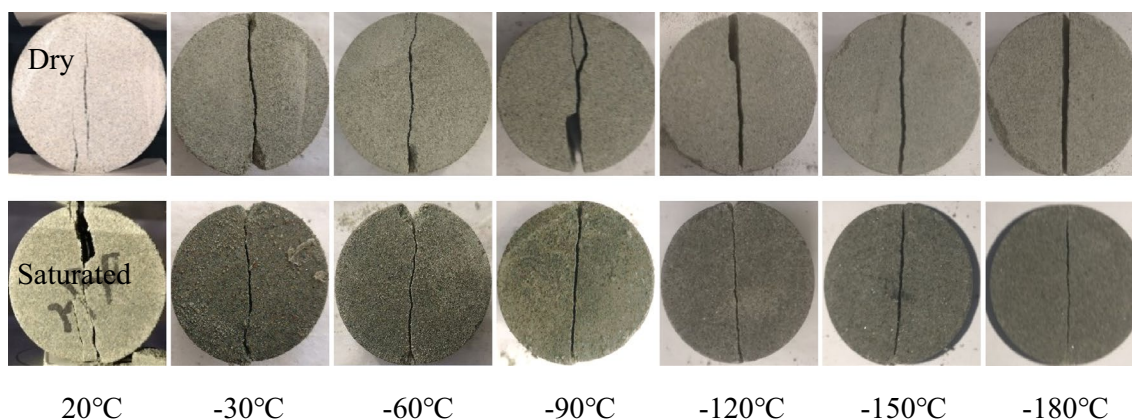


Fig. 16 Brazilian tensile failure patterns of dry (upper row) and saturated (lower row) samples under freezing temperature conditions

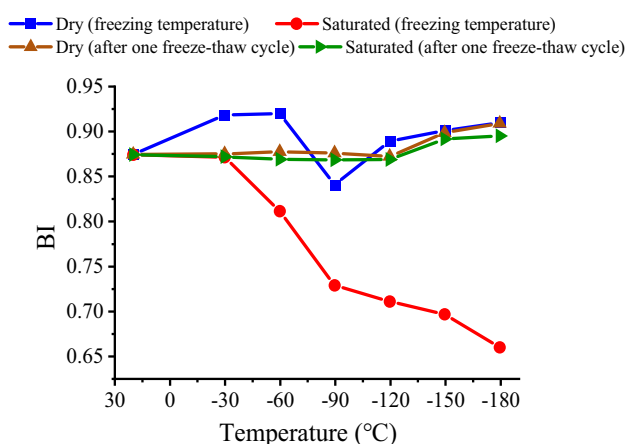


Fig. 17 Variations of sandstone brittleness index with temperature

the characteristics of stress–strain curves and geophysical data, etc. The quantification equation used in this study is shown in Eq. (5).

$$BI = \frac{\sigma_c - \sigma_t}{\sigma_c + \sigma_t} \quad (5)$$

Variations of the brittleness index with temperature are shown in Fig. 17. The brittleness index of dry samples under freezing temperature first increases from 20 to -60 °C, then decreases at -90 °C, followed by an increase until -180 °C, which is similar to the variations of its corresponding UCS, while the brittleness index of saturated sandstones under freezing temperature declines continuously with decreasing temperature from 20 to -180 °C, which is caused by the large increase in tensile strength. The ice filling and cohesion effects significantly increased the sample's resistance to tensile and shear failure, especially at lower temperatures. The formed ice net within the connected pores prevents the quick fracture propagation

and sudden energy release, which is also validated by the less violent failure patterns for the UCS and tensile tests. The brittleness index of saturated samples is always lower than those of dry samples under freezing temperature conditions, and their differences increase as the temperature decreases.

Compared with the freezing temperature test condition, the brittleness index after one freeze–thaw cycle is less affected by the temperature. The brittleness indices of dry and saturated samples after one freeze–thaw cycle remain almost constant at temperatures above -120 °C, while they both increase at -150 °C and -180 °C due to the large damage caused by the freeze and thaw treatment. The brittleness indices of dry samples are only slightly higher than those of saturated samples after one freeze–thaw cycle. The brittleness indices of saturated samples after one freeze–thaw cycle are much higher than those under freezing temperatures at temperatures below -60 °C, while they are lower for dry samples after one freeze–thaw cycle than those under freezing temperature except at -90 °C.

3.3 Effect of Saturation on Rock Mechanical Properties Under Freezing Temperatures

3.3.1 UCS Tests

The stress–strain curves and strains values at different water saturation levels under -120 °C test condition are shown in Fig. 18.

The crack closure strain decreases with the increase in water saturation level, followed by an increase at fully saturated condition. This is because the ice filling reduces the crack compressibility, while new cracks are formed under fully saturated condition due to the volume expansion during the water to ice phase transition. The plastic strain increases with the water saturation as the sample failure process is slowed down by the ice cohesion, while no obvious change

Fig. 18 **a** The stress–strain curves and **b** strain values at different water saturations at $-120\text{ }^{\circ}\text{C}$

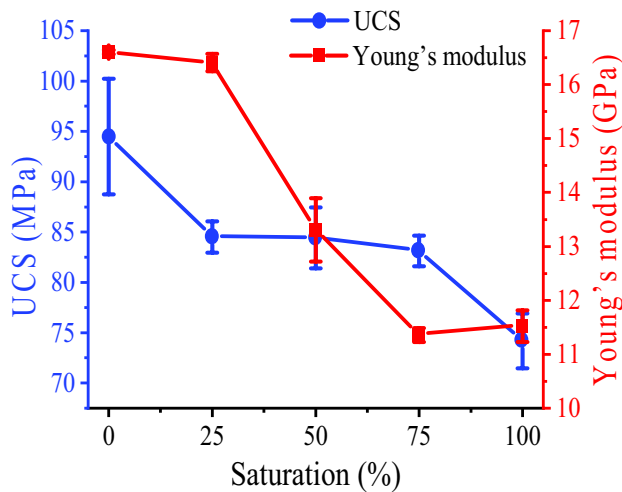
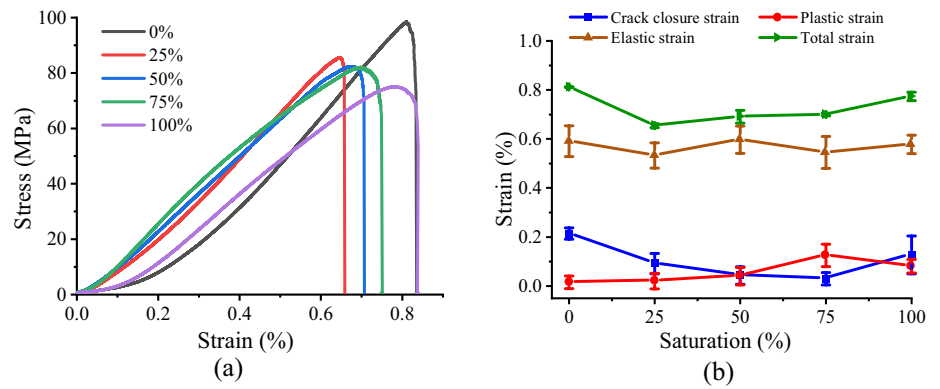


Fig. 19 Variations of UCS and Young's modulus with water saturation at $-120\text{ }^{\circ}\text{C}$

is shown for the elastic strain. The total strain at failure is highest under dry condition as its UCS is largest, while it increases with the water saturation as ice enhances the bearing capacity to deformation. Similarly, the relative standard deviations for total strain are smallest ($<4\%$).

Figure 19 shows the variations of UCS and E with water saturation at $-120\text{ }^{\circ}\text{C}$ with the relative standard deviations being smaller than 6%, and Table 5 summarizes the corresponding mechanisms. As the saturation increases, the compressive strength gradually decreases especially at 25% and 100% water saturation levels. There is a small amount of unfrozen water existing as a film on the mineral surfaces and both the binding water and the ice reduce the friction between grains (Jia et al. 2019). Therefore, the sample strengths are low at partial water saturation conditions. The damage induced by the 9% volume expansion during water to ice phase transition occurs at the fully saturated condition, which results in the strength deterioration. Reductions are also shown for the Young's modulus with the saturation especially between 25 and 75%. The ice filling and bonding effects become more significant with the increase of

Table 5 Effect of water saturation level on mechanical properties at $-120\text{ }^{\circ}\text{C}$

Properties	Change with saturation increase	Mechanisms
Crack closure strain	0–75% decrease 75–100% increase	Ice filling reduces the crack compressibility New cracks formed at full saturation
Elastic strain	Around 0.6%	Remains almost constant
Plastic strain	Increase	Ice cohesion and creep increase plastic deformation
Total strain	0–25% decrease 25–75% increase	UCS decreases significantly Ice increases the sample deformation bearing capacity
UCS	Decrease	(1) The unfrozen water film and ice reduce the friction between grains (2) Damage induced by the 9% volume expansion during water to ice phase transition
Elastic modulus	Decrease	Lower elastic modulus of ice compared with the minerals and the ice creep deformation
BTS	Increase	(1) Cohesion effect of ice (2) Ice in the connected pores acts as fibers
Brittleness index	Decrease	Sample fails in a gentler manner with larger strains as the saturation increases because of the ice cohesion and creep deformation

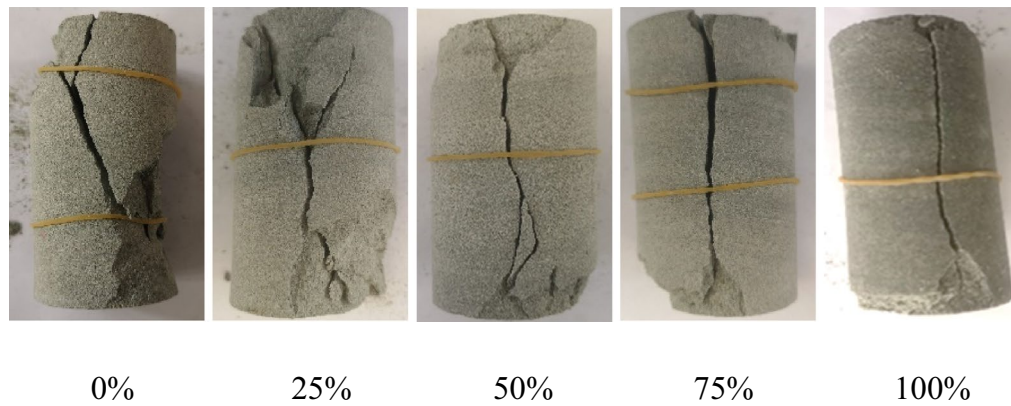


Fig. 20 Sample failure patterns at $-120\text{ }^{\circ}\text{C}$ under different saturations

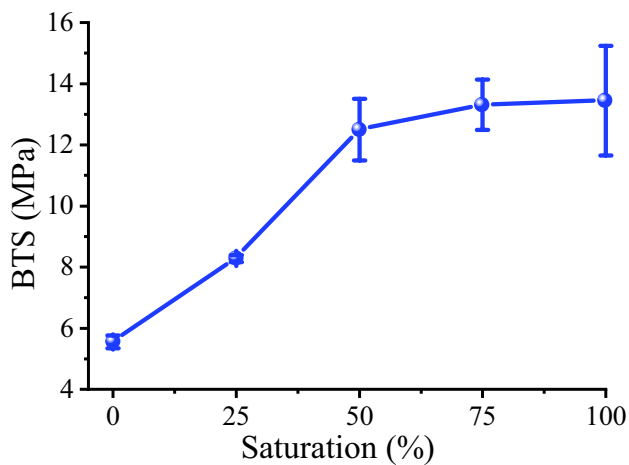


Fig. 21 Tensile strength under different saturation levels at $-120\text{ }^{\circ}\text{C}$

saturation, which is also reflected in the decrease of crack closure strain. However, the lower elastic modulus of ice compared with the minerals and the ice creep deformation result in the reduction of Young's modulus with the ice content.

Figure 20 shows the sample macroscopic fractures after failure with different saturations at $-120\text{ }^{\circ}\text{C}$. Multiple shear fractures are shown for dry and 25% saturated samples, while the number of fractures becomes less and the failure pattern turns to splitting with the increase of water saturation. This failure pattern change is consistent with the variations of the UCS. The higher strength corresponds to larger energy release and more fractures.

3.3.2 Tensile Strength Tests and the Brittleness Index

Figure 21 shows the variations of tensile strength with saturation at $-120\text{ }^{\circ}\text{C}$ with the relative standard deviations smaller than 8% except at full saturation conditions. The tensile strength increases with the water saturation, which is contrary to that of UCS. The tensile strength is 5.55 MPa under dry condition and increases by 142% to 13.46 MPa under fully saturated condition. The significant increase is caused by the cohesion effect of ice, which increases with the saturation. In addition, the ice crystals in the connected pores form a net, which acts as fibers to enhance the tensile strength.

The fracture becomes smoother and less damage occurs at the sample end with the increase of water saturation for

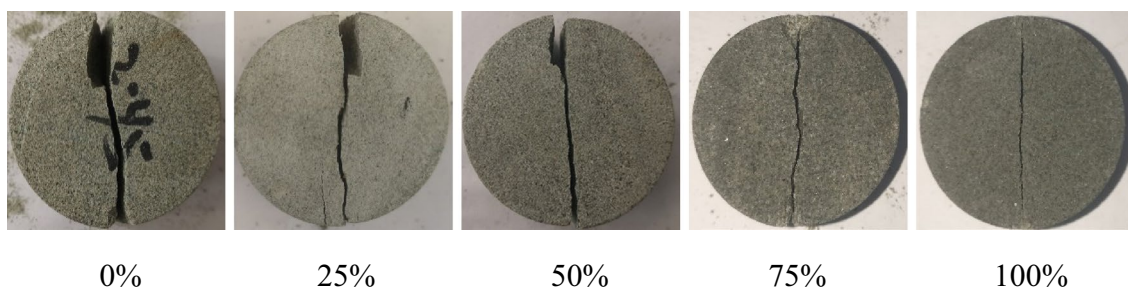


Fig. 22 Failure patterns of Brazilian tensile strength tests under different saturation levels at $-120\text{ }^{\circ}\text{C}$

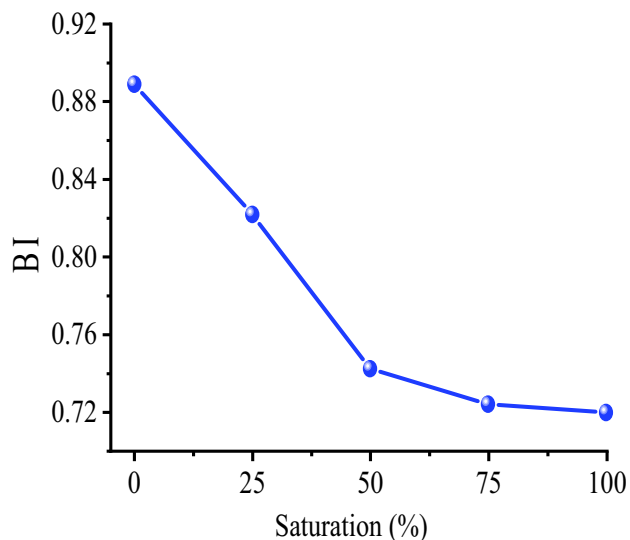


Fig. 23 Variations of brittleness index with saturation at -120 °C

the Brazilian tensile strength tests as shown in Fig. 22, which is consistent with the failure patterns of saturated samples under different freezing temperatures. Bai et al. (2020) also found that the fracture roughness decreases with the increase of tensile strength. The sample defects are gradually filled and cemented by ice with the increase of saturation, which increases the homogeneity and integrity resulting in the fracture extension along the shortest path.

The brittleness index is calculated by Eq. (5), which decreases with the saturation as shown in Fig. 23. The plastic deformation increases, while the Young’s modulus decreases with the water saturation under UCS tests, which are related to the ice cohesion and creep deformation. Therefore, the sample fails in a gentler manner with larger strains as the saturation increases. The less complicated fractures in the UCS and Brazilian tensile strength tests at higher saturation levels also indicate that the failure is

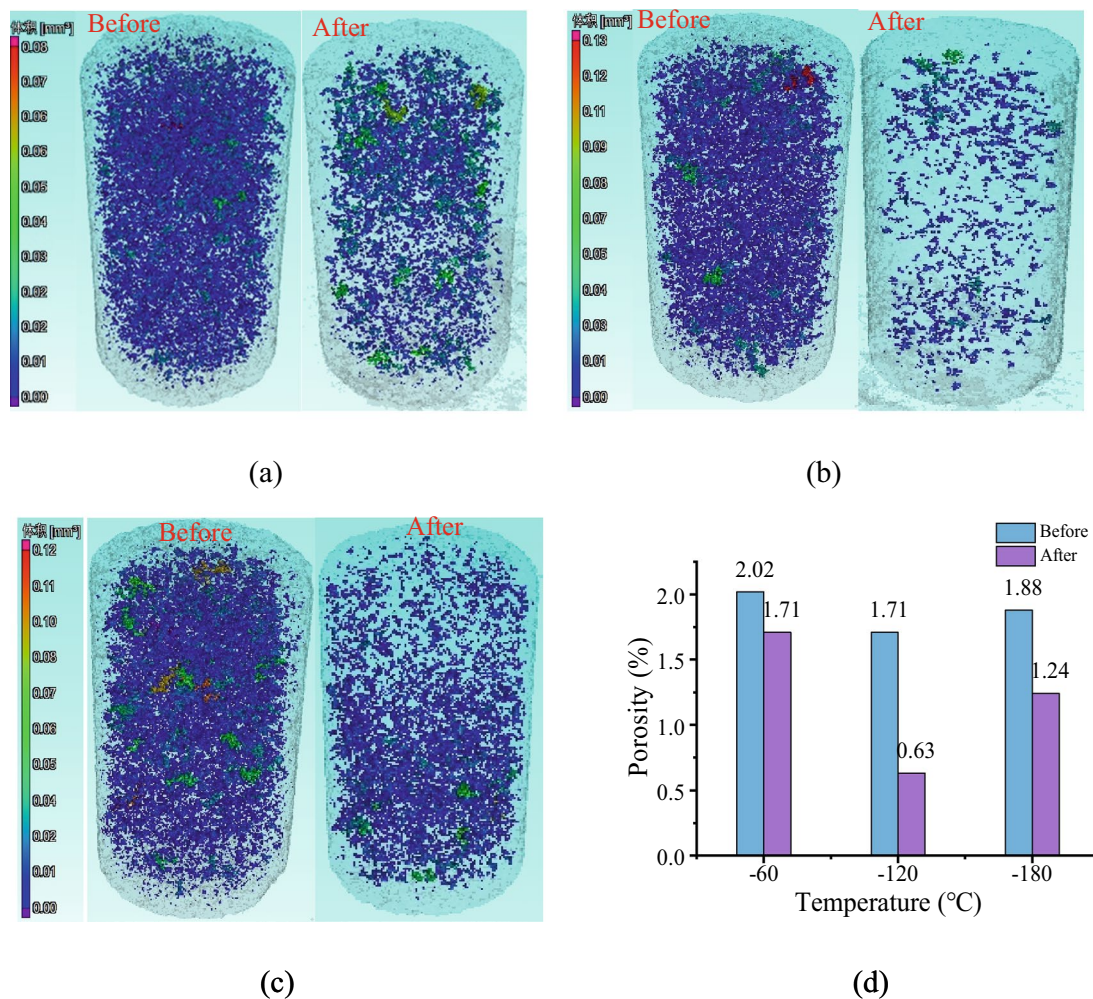


Fig. 24 Pore changes of saturated samples before and after the ultralow temperature freeze-thaw cycle treatments at -60 °C a; -120 °C b; -180 °C c and porosity d, respectively

more moderate and the brittleness index is lower under large ice content.

3.4 Microscopic Observations After Ultralow Temperature Freeze–Thaw Cycle Treatment

Figure 24 shows the comparisons of CT images and total porosities of saturated sandstones before and after the ultralow temperature freeze–thaw cycle treatments at $-60\text{ }^{\circ}\text{C}$, $-120\text{ }^{\circ}\text{C}$ and $-180\text{ }^{\circ}\text{C}$, respectively. Obvious reductions in the number of pores and porosity after the ultralow temperature freeze–thaw cycle treatments are shown. It should be noted that the nanopores cannot be detected by the CT scanning due to the resolution limitations; therefore, the calculated porosities are much smaller than that in the mercury intrusion porosity tests. The porosity is lowest with the largest reduction after the $-120\text{ }^{\circ}\text{C}$ treatment, which is consistent with that the UCS of saturated sample after the ultralow temperature freeze–thaw cycle treatment is highest at $-120\text{ }^{\circ}\text{C}$ compared with those at $-60\text{ }^{\circ}\text{C}$ and $-180\text{ }^{\circ}\text{C}$. The incongruous shrinkage and expansion of different minerals during the freeze–thaw cycle induce the relative movement between grains. In addition, the volume expansion and shrinkage during water–ice phase transitions induce damages near the large pores. The lower resistance of pre-existing large pores and fractures result in the inward deformation, and the debris from the cement destruction will also fill the large defects, which is certified by the SEM images shown below. Though small cracks are created between the grain boundaries, they are undetectable by the CT. Therefore, the filling of large pores results in the reduction of porosity. As the temperature variation for $-120\text{ }^{\circ}\text{C}$ treatment is larger than that at $-60\text{ }^{\circ}\text{C}$, the pore filling is more significant resulting in the lower porosity. While the larger freeze–thaw damage at $-180\text{ }^{\circ}\text{C}$ induces the cracking which increases the porosity. As a result, the porosity is lowest at $-120\text{ }^{\circ}\text{C}$ compared with $-60\text{ }^{\circ}\text{C}$ and $-180\text{ }^{\circ}\text{C}$. Though porosity becomes lower after the ultralow temperature freeze–thaw cycle treatment, the cohesion and internal structures are destroyed resulting in the lower UCS values compared with that at $20\text{ }^{\circ}\text{C}$.

The porosity increases after freeze–thaw cycles as reported in the literature are not shown in this study. This is because only one freeze–thaw cycle was conducted for our tests and the initial sample was intact with a low porosity of 8.38%; therefore, the damage is small and is characterized by the plastic deformation toward the defects. Besides, the induced small cracks at grain boundaries are not counted due to the resolution limitations of CT. Zhang et al. (2020) also found the rock porosities at some cross sections were reduced after 5 freeze–thaw cycles. Zheng et al. (2019) demonstrated that

porosity reductions and increases of longitudinal wave velocity were shown at small numbers of freeze–thaw cycles, then the porosity gradually increased and the wave velocity decreased with the increase of freeze–thaw cycles. It is expected that the porosity will increase if more freeze–thaw cycles are conducted for our samples, as the internal damage is induced resulting in lower resistance to the ice expansion force.

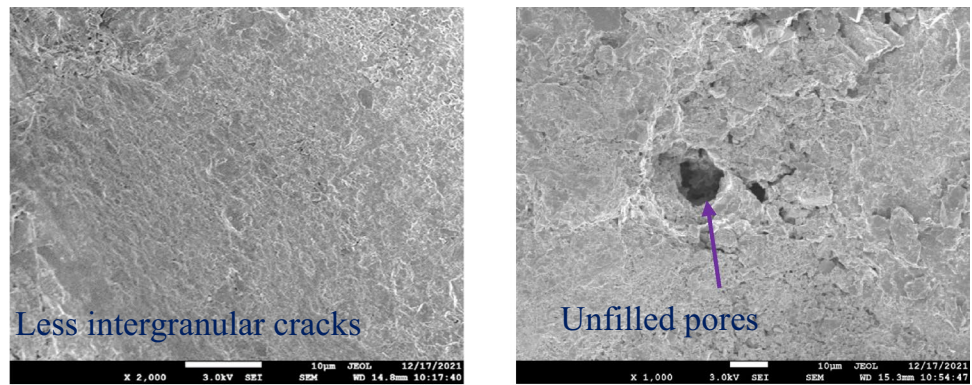
Figure 25 shows the SEM images of saturated sandstone before and after the ultralow temperature treatment at $-150\text{ }^{\circ}\text{C}$. Less intergranular cracks are shown and pores are unfilled before thermal treatments as shown in Fig. 25a. Cracks are formed at the grain boundaries after the freeze–thaw cycle, which is due to the differences in the mineral thermal expansion coefficients. There are many damaged areas near the original defects, as the phase transitions between water and ice mainly occur in the pores and fractures inducing further damage. Pore and crack fillings are shown due to the cementation destruction and the relative movement between grains, which result in porosity reduction.

4 Conclusions

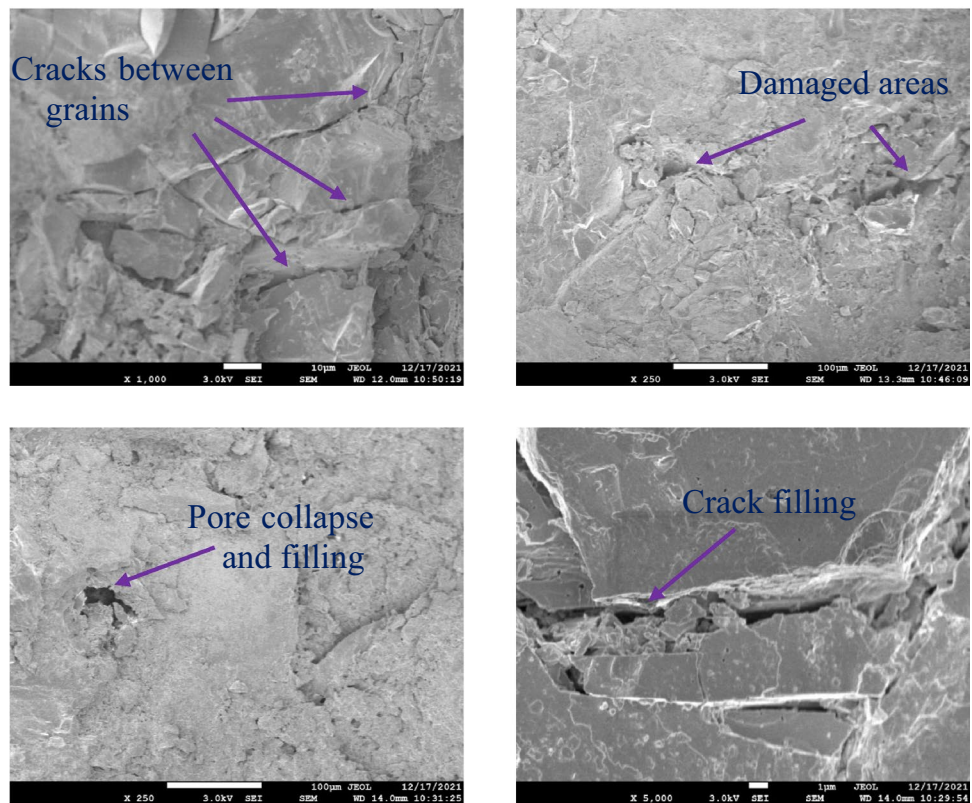
The influences of temperature and saturation on the mechanical properties for Zigong sandstone samples under the freezing temperature and after one freeze–thaw cycle test conditions (-30 to $-180\text{ }^{\circ}\text{C}$) are investigated by UCS and Brazilian tensile strength tests. The characteristics of stress–strain curves, strengths, failure patterns and brittleness under different conditions are analyzed. The microscopic changes in the saturated samples after the freeze–thaw cycle were studied by CT and SEM observations. The main conclusions are as follows.

- (1) The UCS of dry samples are always higher than those of saturated samples and are also larger under the freezing temperature than those after one freeze–thaw cycle. The Young's modulus of saturated samples is lower than its dry counterpart. The Young's modulus of saturated samples under freezing temperature is smaller than that after one freeze–thaw cycle and continuously decreases with the reduction of temperature due to the higher ice content. In general, the crack closure strain decreases, while the elastic strain increases with the decrease of temperature.
- (2) The tensile strength of saturated samples under freezing temperature increases with the decrease of temperature, as the ice content and strength increase as the temperature decreases. In addition, the formed ice net in connected pores acts as fiber to enhance the tensile strength, while the tensile strengths of dry samples

Fig. 25 SEM images of sandstone before **a** and after **b** thermal treatment at $-150\text{ }^{\circ}\text{C}$



(a)



(b)

are higher than those of saturated samples after one freeze–thaw cycle, which is caused by the water softening effects and the damage induced by the water–ice phase transitions.

- (3) The UCS failure pattern of dry samples under freezing temperature changes from diagonal shear at $20\text{ }^{\circ}\text{C}$ to X -type shear at $-150\text{ }^{\circ}\text{C}$ and $-180\text{ }^{\circ}\text{C}$, while vertical splitting dominates at freezing temperatures for saturated samples as the filling and bonding effects of ice increase the sample homogeneity. Bifurcations occur

- in the tensile strength tests for dry sample with high strengths under freezing temperature, while the damaged area becomes smaller and the fracture becomes smoother with the decrease of temperature for saturated samples. The brittleness indexes of dry samples are higher than those of saturated samples under freezing temperature, which is also verified by the more complex fracture morphologies for dry samples.
- (4) For tests of samples with different saturations at $-120\text{ }^{\circ}\text{C}$, the closure strain decreases with the satura-

tion except under fully saturated condition, while the plastic strain increases with the saturation. Both UCS and Young's modulus decrease with saturation, while the tensile strength increases with saturation. The brittleness index decreases with the saturation, and failure patterns become less destructive with the increase of saturation.

- (5) The porosity of saturated samples measured by CT reduces after the one freeze–thaw cycle. The porosity is lowest after the treatment at $-120\text{ }^{\circ}\text{C}$ compared with those at $-60\text{ }^{\circ}\text{C}$ and $-180\text{ }^{\circ}\text{C}$. Pore filling resulting from the movement of grains and debris toward the defects induces porosity reduction, which is also indicated by the SEM images.

Acknowledgements The authors would like to acknowledge the financial support from the Natural Science Foundation of Hebei Province (E2020202170), Natural Science Foundation of China (42202325, 42172306) Top Young Talents Program of Department of Education of Hebei Province (BJ2021022) and Hebei Province (No. 2020HBQZYC001).

Data availability The experimental data can be provided upon request.

Declarations

Conflict of interest The authors declare that they have no known competing financial interests or personal relationships that could have appeared to influence the work reported in this paper.

References

- Arakawa M, Maeno N (1997) Mechanical strength of polycrystalline ice under uniaxial compression. *Cold Reg Sci Technol* 26(3):215–229
- Bai Y, Shan R, Ju Y, Wu Y, Sun P, Wang Z (2020) Study on the mechanical properties and damage constitutive model of frozen weakly cemented red sandstone. *Cold Regions Sci Technol* 2020:171
- Cai CZ, Li GS, Huang ZW, Shen ZH, Tian SC, Wei JW (2014a) Experimental study of the effect of liquid nitrogen cooling on rock pore structure. *J Nat Gas Sci Eng* 21:507–517
- Cai CZ, Li GS, Huang ZW, Shen ZH, Wang HZ, Tian SC, Wei JW (2014b) Experiment study of rock porous structure damage under cryogenic nitrogen freezing. *Rock Soil Mech* 35(4):965–971
- Chen TC, Yeung MR, Mori N (2004) Effect of water saturation on deterioration of welded tuff due to freeze–thaw action. *Cold Reg Sci Technol* 38(2–3):127–136
- Chung SK, Han KC, Park ES (2006) Feasibility study of underground LNG storage system in rock cavern. *Tunnel Undergr Space* 16(4):296–306
- Feng Q, Jiang BS, Zhang Q, Wang LP (2014) Analytical elasto-plastic solution for stress and deformation of surrounding rock in cold region tunnels. *Cold Reg Sci Technol* 108:59–68
- Feng Q, Jin J, Zhang S, Liu W, Yang X, Li W (2022) Study on a damage model and uniaxial compression simulation method of frozen–thawed rock. *Rock Mech Rock Eng* 55(1):187–211
- Haynes FD (1980) Temperature effect on the uniaxial strength of ice. In: International conference on port and ocean engineering under arctic conditions. Trondheim, Norway (CONF-790833)
- He T, Chong ZR, Zheng J, Ju Y, Linga P (2019) LNG cold energy utilization: prospects and challenges. *Energy* 170(2):557–568
- Huang S, Ye Y, Cui X, Cheng A, Liu G (2020) Theoretical and experimental study of the frost heaving characteristics of the saturated sandstone under low temperature. *Cold Regions Sci Technol* 2020:174
- Inada Y, Yokota K (1984) Some studies of low temperature rock strength. *Int J Rock Mech Min Sci Geomech Abstr* 21(3):145–153
- Ji SY, Wang AL, Su J, Yue QJ (2011) Experimental studies on elastic modulus and flexural strength of sea ice in the Bohai Sea. *J Cold Regions Eng* 25(4):182–195
- Jia H, Liu Q, Xiang W, Zhang W, Lang L (2013) Damage evolution model of saturated sandstone under freeze–thaw cycles. *Chin J Rock Mech Eng* 32(S2):3049–3055
- Jia H, Xiang W, Tan L, Zhang W, Zeng W, Cao S, Cheng C (2016) Theoretical analysis and experimental verifications of frost damage mechanism of sandstone. *Chin J Rock Mech Eng* 35(5):879–895
- Jia HL, Zi F, Yang GS, Li GY, Shen YJ, Sun Q, Yang PY (2019) Influence of pore water (ice) content on the strength and deformability of frozen argillaceous siltstone. *Rock Mech Rock Eng* 53(2):967–974
- Jia HL, Ding S, Zi F, Dong YH, Shen YJ (2020) Evolution in sandstone pore structures with freeze–thaw cycling and interpretation of damage mechanisms in saturated porous rocks. *CATENA* 195:104915
- Kammoshida N, Okawara M, Abe M, Furuzumi M (2010) Mechanical behavior of Kimachi sandstone under ultralow temperature. *J Min Mater Process Inst Jpn* 127(1):8–13
- Kodama J, Goto T, Fujii Y, Hagan P (2013) The effects of water content, temperature and loading rate on strength and failure process of frozen rocks. *Int J Rock Mech Min Sci* 62:1–13
- Kurilko A, Novopashin M (2005) Features of low temperature effect upon strength of enclosing rock and kimberlite in the “Udachnaya” pipe. *J Min Sci* 41(2):119–122
- Lemaitre J (1985) A continuous damage mechanics model for ductile fracture. *J Eng Mater Technol* 107(1):83–89
- Li YP, Wang ZY (2012) Study of parameters and strength of thermal effects for granite under low temperature. *Rock Soil Mech* 33(2):321–325
- Li ZF, Xu HF, Zhang CY (2016) Liquid nitrogen gasification fracturing technology for shale gas development. *J Petrol Sci Eng* 138:253–256
- Liu M, Bai B, Li X (2014) Experimental studies on the short term effect of CO_2 on the tensile failure of sandstone. *Energy Proc* 63:3357–3363
- Looney B (2021) Statistical review of world energy globally consistent data on world energy markets and authoritative publications in the field of energy. *Rev World Energy Data* 70:8–20
- Ma Z, Zhang G, Gamage RP, Zhang C (2021) Measurement of thermal expansion coefficient of rock minerals using XRD and its implications to thermal damage mechanism. *IOP Conf Ser Earth Environ Sci* 861(7):1
- Mardoukhi A, Mardoukhi Y, Hokka M, Kuokkala V-T (2020) Effects of test temperature and low temperature thermal cycling on the dynamic tensile strength of granitic rocks. *Rock Mech Rock Eng* 54(1):443–454
- Matsunaga I, Kuriyagawa M, Kinoshita N (1981) Mechanical properties of rock at cryogenic temperature. *J Min Mater Process Inst Jpn* 97:431–436
- Memon KR, Mahesar AA, Ali M, Tunio AH, Mohanty US, Akhondzadeh H, Awan FUR, Iglauer S, Keshavarz A (2020) Influence of cryogenic liquid nitrogen on petro-physical

- characteristics of mancos shale: an experimental investigation. *Energy Fuels* 34(2):2160–2168
- Ming F, Zhang S, Niu F, Zhou Z (2021) A study on crack damage stress and the damage constitutive model of frozen sandstone. *Bull Eng Geol Env* 80(9):6955–6970
- Ning JG, Wang H, Zhu ZW, Sun YX (2005) Investigation of the constitutive model of frozen soil based on meso-mechanics. *J Beijing Inst Technol* 2005:10
- Sammis C, Biegel R (2004) Mechanics of strengthening in crystalline rock at low temperatures: a preliminary assessment. In: *Proceedings of the 26th seismic research review: trends in nuclear explosion monitoring*, pp 475–484
- Song YQ, Liu JC, Shao ZX (2020) Experimental study on physical and mechanical properties of limestone under freezing thawing cycles. *Sci Technol Eng* 20(2):741–746
- Tang M, Wang Z, Sun Y, Ba J (2010) Experimental study of mechanical properties of granite under low temperature. *Chin J Rock Mech Eng* 29(4):787–794
- Ulusay R (2015) The ISRM suggested methods for rock characterization, testing and monitoring: 2007–2014. *Int J Rock Mech Min Sci* 46:627–634
- Wan D, Zhu Z, Zhou C, Li J, Ying P, Wang M (2020) Effect of pre-existing symmetrical cracks on propagation behaviors of a blast-induced crack. *Shock Vib* 2020:1
- Wang L, Lu Z, Shao S (2017) A composite power exponential nonlinear model of rock and soil. *Chin J Rock Mech Eng* 39(9):1724–1730
- Wang EL, Ren ZF, Han HW (2021) Experimental study on uniaxial compressive strength of ultra-low temperature frozen clay. *Chin J Geotech Eng* 43(10):1851–1860
- Weibull W (1951) A statistical distribution function of wide applicability. *J Appl Mech* 18(3):293–297
- Xie Q, Zhu Z, Kang G (2014) Dynamic stress–strain behavior of frozen soil: experiments and modeling. *Cold Reg Sci Technol* 106–107:153–160
- Xu B, Li N, Li ZK, Yan N (2013) Low-temperature LPG and LNG storage caverns and related research review of rock mechanics. *Chin J Rock Mech Eng* 32(S2):2977–2993
- Zhang D, Ranjith PG, Perera MSA (2016) The brittleness indices used in rock mechanics and their application in shale hydraulic fracturing: a review. *J Petrol Sci Eng* 143:158–170
- Zhang D, Pathegama Gamage R, Perera M, Zhang C, Wanniarachchi W (2017) Influence of water saturation on the mechanical behaviour of low-permeability reservoir rocks. *Energies* 10(2):236
- Zhang HM, Wang H, Zhang JF (2020) Analysis of meso-damage characteristics of freeze–thaw rock on CT scale. *J Liaoning Tech Univ (nat Sci)* 39(1):51–56
- Zhao J, Xie M, Yu J, Zhao W (2019) Experimental study on mechanical properties and damage evolution of fractured rock under freezing–thawing action. *J Eng Geol* 27(6):1199–1207
- Zheng GH, Xu JY, Wang P, Fang XY, Wen M (2019) Physical characteristics and degradation model of stratified sandstone under freeze–thaw cycling. *Rock Soil Mech* 40(02):632–641
- Zhu YL, Zhang JY (1992) Constitutive relations of frozen soil in uniaxial compression. *J Glaciol Geocryol* 14(3):210–217

Publisher's Note Springer Nature remains neutral with regard to jurisdictional claims in published maps and institutional affiliations.

Springer Nature or its licensor (e.g. a society or other partner) holds exclusive rights to this article under a publishing agreement with the author(s) or other rightsholder(s); author self-archiving of the accepted manuscript version of this article is solely governed by the terms of such publishing agreement and applicable law.